*The Canadian Mineralogist*
Vol. 52, pp. 337-350 (2014)
DOI: 10.3749/canmin.52.2.337

# CRYSTAL CHEMISTRY OF SYNTHETIC $M^{2+}Be_2P_2O_8$ ($M^{2+}$ = Ca, Sr, Pb, Ba) BERYLLOPHOSPHATES

FABRICE DAL BO, FRÉDÉRIC HATERT[§], AND MAXIME BAIJOT

*Laboratoire de Minéralogie, B18, Université de Liège, B-4000 Liège, Belgium*

## ABSTRACT

Four beryllophosphates with general formula $M^{2+}Be_2P_2O_8$ ($M^{2+}$ = Ca, Sr, Pb, Ba) have been synthesized under hydrothermal conditions at 200 °C. Their crystal structures were solved by direct methods and refined by full-matrix least-squares techniques on the basis of $F^2$ for all unique reflections to agreement indices $R_1$ of 2.3, 4.8, 1.5, and 2.1%, respectively. $CaBe_2P_2O_8$ is monoclinic, space group $P2_1/c$, $Z = 4$, $a$ 7.809(1), $b$ 8.799(1), $c$ 8.309(1) Å, β 90.51(1)°, $V$ 570.98(2) Å$^3$. $SrBe_2P_2O_8$ is monoclinic, space group $P2_1/c$, $Z = 4$, $a$ 8.000(1), $b$ 8.986(1), $c$ 8.418(1) Å, β 90.22(1)°, $V$ 605.10(6) Å$^3$. $PbBe_2P_2O_8$ is monoclinic, space group $P2_1/c$, $Z = 4$, $a$ 8.088(1), $b$ 9.019(1), $c$ 8.391(1) Å, β 90.12(1)°, $V$ 612.22(1) Å$^3$. $BaBe_2P_2O_8$ is hexagonal, space group $P6/mmm$, $Z = 1$, $a$ 5.028(1), $c$ 7.466(1) Å, $V$ 162.51(1) Å$^3$. The three first compounds are isostructural and show a paracelsian-type structure composed of a framework of corner-sharing $BeO_4$ and $PO_4$ tetrahedra. These tetrahedra are assembled in four- and eight-membered rings showing the typical UUDD and DDUDUUDU patterns, respectively. The $M^{2+}$ (Ca, Sr, Pb) cation occurs in a distorted 7+3-coordinated polyhedron located in the eight-membered ring. $CaBe_2P_2O_8$ and $SrBe_2P_2O_8$ are isostructural with the minerals hurlbutite and strontiohurlbutite, respectively. The structure of $BaBe_2P_2O_8$ consists of double layers of tetrahedra, which contain both Be and P in a 1:1 ratio. Inside the layers, the $(Be,P)O_4$ tetrahedra form six-membered rings by sharing corners. The Ba atoms are located in very regular 12-coordinated polyhedra and connect two successive double layers. This Ba beryllophosphate is the synthetic counterpart of minjiangite, and shows similarities with the mineral dmisteinbergite, $CaAl_2Si_2O_8$, a hexagonal polymorph of anorthite. Other hydrothermal experiments were performed in order to establish the stability of these $M^{2+}Be_2P_2O_8$ compounds as a function of temperature and pH; the results show that synthetic hurlbutite can crystallize in acidic as well as in basic conditions. Furthermore, these experiments show that the four title compounds are stable at high temperatures and pressures (600 °C, 1 kbar).

*Keywords:* beryllophosphates, hydrothermal synthesis, crystal chemistry, paracelsian-type structure

## INTRODUCTION

Only 27 natural beryllophosphates are reported in the literature, occurring mainly in granitic pegmatites and resulting from the reaction of beryl with P-bearing hydrothermal solutions (Kampf 1992, Černý 2002). The formation of these minerals is highly dependent upon the pH, temperature, availability of specific alkali cations, and Be:P ratio of the solution (Kampf *et al.* 1992). Despite their low abundance, beryllophosphate minerals crystallize in many structure types, characterized by different polymerization degrees of the $BeO_4$-$PO_4$ tetrahedra; these compounds form chain structures [fransoletite $Ca_3Be_2(PO_4)_2(PO_3OH)_2{\cdot}4H_2O$, väyrynenite, $MnBe(PO_4)(OH)$], sheet structures [herderite, $CaBe(PO_4)(F,OH)$, uralolite, $Ca_2Be_4(PO_4)_3(OH)_3{\cdot}5H_2O$], framework structures [hurlbutite, $CaBe_2P_2O_8$, babefphite, $BaBe(PO_4)F$, beryllonite, $NaBe(PO_4)$], structures containing clusters of tetrahedra [gainesite, $Na_2BeZr_2(PO_4)_4{\cdot}1.5H_2O$], and even zeolite-type structures [pahasapaite, $Li_8(Ca,Li,K)_{10.5}Be_{24}(PO_4)_{24}{\cdot}38H_2O$] (Hawthorne & Huminicki 2002). To date, structural data are still missing for two natural beryllophosphate minerals: faheyite, $MnFe^{3+}{}_2Be_2(PO_4)_4{\cdot}6H_2O$ (Lindberg & Murata 1953), and glucine, $CaBe_4(PO_4)_2(OH)_4{\cdot}0.5H_2O$ (Grigoriev 1963).

The crystal chemistry of the beryllophosphates is exciting, as their structures are similar to those of aluminosilicates and borosilicates. For example, hurlbutite is topologically identical to danburite, $CaB_2Si_2O_8$ (Phillips *et al.* 1974); herderite is isostructural with datolite, $CaBSiO_4(OH)$ (Foit *et al.* 1973), and bergslagite, $CaBeAsO_4(OH)$ (Hansen *et al.* 1984); pahasapaite is topologically similar to the minerals of the faujasite group, $(Ca,Na,Mg)_5(Si,Al)_{12}O_{24}{\cdot}15H_2O$ (Pluth & Smith 1972); and tiptopite, $K_2(Li,Na,Ca)_6(Be_6P_6)$

§ *Corresponding author e-mail address*: fhatert@ulg.ac.be

$O_{24}(OH)_2 \cdot 1.3H_2O$ (Peacor *et al.* 1987), is isotypic with the minerals of the cancrinite group, $(Na,Ca)_8(Al_6Si_6)O_{24}(CO_3,SO_4)_2 \cdot 2H_2O$. All these analogies can be explained by the Pauling bond-valance rule. Indeed, the O atoms shared by Be and P in beryllosphosphates, by Al and Si in aluminosilicates, and by B and Si in borosilicates receive exactly the same Pauling bond-valence sum of 1.75 (Kampf 1992).

## Experimental Procedure

### *Hydrothermal synthesis*

The single crystals of beryllophosphates used for this study were synthesized under hydrothermal conditions. Mixtures of BeO, $H_3PO_4$ (85%), $NH_4H_2PO_4$, $CaHPO_4$, $Sr(NO_3)_2$, $Pb(NO_3)_2$, $Ba(OH)_2.8H_2O$ (Table 1), and ultra-pure water (2 mL) were heated in a Parr 23-mL autoclave with PTFE liner. The autoclave was then placed in a furnace and maintained at 200 °C for seven days under autogeneous pressure. After rapid cooling to room temperature (50 °C/h), the resulting products were recovered by filtration and washed with distilled water. When necessary, the pH of the solution was measured before and after heating the starting material.

Colorless crystals of $CaBe_2P_2O_8$ (*CaBeP*), $SrBe_2P_2O_8$ (*SrBeP*), and $PbBe_2P_2O_8$ (*PbBeP*) are generally small and reach 0.1 mm in length; the colorless crystals of $BaBe_2P_2O_8$ (*BaBeP*) can attain more than 2 mm in length and form perfect hexagonal tablets. The single crystals used for the structure refinements were selected from experiments CaBeP200-1, SrBeP200-3, PbBeP200-1, and BaBeP200-1.

High-temperature hydrothermal experiments were also performed, using the synthetic products obtained in experiments CaBeP200-1, SrBeP200-3, PbBeP200-1, and BaBeP200-1 (Table 1). About 25 mg of each starting material was crushed and sealed into gold tubes with an outer diameter of 2 mm and a length of 25 mm, containing 2 μL of distilled water. The gold capsules were then inserted into a Tuttle-type pressure vessel (Tuttle 1949) and maintained at temperatures of 400 and 600 °C, under a pressure of 0.1 GPa. After seven days, the gold tubes containing the sample were quenched to room temperature in the autoclave in a stream of cold air.

### *X-ray diffraction*

The synthesized compounds were identified by X-ray powder diffraction, with a Panalytical PW 3710 diffractometer using Fe*K*α radiation (λ = 1.9373 Å, 40 kV, 30 mA). Single-crystal X-ray diffraction measurements were performed with an Agilent Technologies Xcalibur four-circle diffractometer (kappa geometry), using Mo*K*α radiation (λ = 0.7107 Å, 40 kV, 40 mA), and equipped with an EOS CCD area detector. A summary of crystal data is presented in Table 2. The

TABLE 1. HYDROTHERMAL SYNTHESIS PERFORMED IN THE $M^{2+}$–Be–$PO_4$ SYSTEM

| N° sample | BeO (mg) | $CaHPO_4$ (mg) | $Sr(NO_3)_2$ (mg) | $Pb(NO_3)_2$ (mg) | $Ba(OH)_2.8H_2O$ (mg) | $NH_4H_2PO_4$ (mg) | $H_3PO_4$ (mL) | T (°) | Time (days) | Synthesized compounds |
|---|---|---|---|---|---|---|---|---|---|---|
| CaBeP200-1 | 101 | 203 | - | - | - | - | 2 | 200 | 7 | $CaBe_2P_2O_8$ |
| CaBeP200-2 | 50 | 400 | - | - | - | - | 2 | 200 | 7 | $CaBe_2P_2O_8$ |
| CaBeP200-3 | 100 | 136 | - | - | - | - | 0.07 | 200 | 7 | $CaBe_2P_2O_8$, BeO |
| CaBeP200-4 | 50 | 408 | - | - | - | - | 0.07 | 200 | 7 | $CaBe_2P_2O_8$ |
| CaBeP150-5 | 100 | 271 | - | - | - | - | 0.07 | 150 | 7 | $CaBe_2P_2O_8$ |
| CaBeP200-7 | 50 | 407 | - | - | - | 115 | - | 200 | 7 | $CaBe_2P_2O_8$, $Ca_5(PO_4)_3(OH)$ |
| CaBeP200-8 | 100 | 135 | - | - | - | 115 | - | 200 | 7 | $CaBe_2P_2O_8$, $Ca_5(PO_4)_3(OH)$ |
| SrBeP200-1 | 25 | - | 212 | - | - | 117 | - | 200 | 7 | $SrBe_2P_2O_8$, $Sr(HPO_4)$, BeO |
| SrBeP200-2 | 100 | - | 211 | - | - | 230 | - | 200 | 7 | $SrBe_2P_2O_8$, BeO |
| SrBeP200-3 | 100 | - | 212 | - | - | - | 2 | 200 | 7 | $SrBe_2P_2O_8$ |
| PbBeP200-1 | 162 | - | - | 331 | - | - | 2 | 200 | 7 | $PbBe_2P_2O_8$ |
| BaBeP200-1 | 150 | - | - | - | 315 | - | 2 | 200 | 7 | $BaBe_2P_2O_8$ |
| CaBeP400 | Products of the CaBeP200-1 experiment used as starting materials | | | | | | | 400 | 7 | $CaBe_2P_2O_8$ |
| CaBeP600 | | | | | | | | 600 | 7 | $CaBe_2P_2O_8$ |
| SrBeP400 | Products of the SrBeP200-3 experiment used as starting materials | | | | | | | 400 | 7 | $SrBe_2P_2O_8$ |
| SrBeP600 | | | | | | | | 600 | 7 | $SrBe_2P_2O_8$ |
| PbBeP400 | Products of the PbBeP200-1 experiment used as starting materials | | | | | | | 400 | 7 | $PbBe_2P_2O_8$ |
| PbBeP600 | | | | | | | | 600 | 7 | $PbBe_2P_2O_8$ |
| BaBeP400 | Products of the BaBeP200-1 experiment used as starting materials | | | | | | | 400 | 7 | $BaBe_2P_2O_8$ |
| BaBeP600 | | | | | | | | 600 | 7 | $BaBe_2P_2O_8$ |

single-crystal intensity data were corrected for Lorenz, polarization, and absorption effects, the latter with an empirical method using the SCALE3 ABSPACK scaling algorithm included in the CrysAlisRED package (Agilent 2012). The structures were solved by direct methods using SHELXS, and then refined with SHELXTL (Sheldrick 2008); scattering curves for neutral atoms, together with anomalous dispersion corrections, were taken from the *International Tables for X-ray Crystallography, Vol. C* (Wilson 1992). The refinements were completed using anisotropic-displacement parameters for all atoms. Positional and displacement parameters are given in Table 3, and interatomic distances and angles are given in Table 4. Refined site occupancies for *CaBeP*, *SrBeP*, and *PbBeP* showed that all crystallographic sites are fully occupied; consequently, all sites were constrained to full occupancy in the final refinement cycles.

### *Infrared Spectroscopy*

The infrared spectra of the four synthetic compounds (Fig. 1) were recorded using a Nicolet NEXUS spectrometer, from 32 scans with a 1 $cm^{-1}$ resolution, over the 400-4000 $cm^{-1}$ region. The samples were prepared by intimately mixing 2 mg of sample with KBr, in order to obtain a 150 mg homogeneous pellet, which was subsequently dried for a few hours at 110 °C. To prevent water contamination, the measurements were performed under a dry air purge.

## Crystal Structure Descriptions

The observed X-ray powder-diffraction pattern of $CaBe_2P_2O_8$ is identical to that of natural hurlbutite (Lindbloom *et al*. 1974); those of $SrBe_2P_2O_8$ and $PbBe_2P_2O_8$ are also similar, but show a significant displacement of the diffraction peaks toward higher *d* values. The X-ray powder-diffraction pattern of $BaBe_2P_2O_8$ shows similarities with that of dmisteinbergite, $CaAl_2Si_2O_8$, a hexagonal polymorph of anorthite (Takéuchi & Donnay 1959). Note that $SrBe_2P_2O_8$ and $BaBe_2P_2O_8$ were already present in the ICDD data base, but their crystal structures were not provided (International Center for Diffraction Data, PDF card 00-026-0977 and 00-026-0140, respectively). The X-ray powder diffraction patterns indicate that the final synthesized compounds were completely crystallized (no amorphous phase) and exclusively composed of the beryllophosphates reported in the present study.

### *$CaBe_2P_2O_8$, $SrBe_2P_2O_8$, and $PbBe_2P_2O_8$*

The compounds $CaBe_2P_2O_8$, $SrBe_2P_2O_8$, and $PbBe_2P_2O_8$ crystallized in the same space group ($P2_1/c$) and are isostructural. Moreover, $CaBe_2P_2O_8$ and

TABLE 2. SINGLE-CRYSTAL DIFFRACTION DATA AND REFINEMENT PARAMETERS

| | $CaBe_2P_2O_8$ | $SrBe_2P_2O_8$ | $PbBe_2P_2O_8$ | $BaBe_2P_2O_8$ |
|---|---|---|---|---|
| *a* (Å) | 7.809(1) | 8.000(1) | 8.088(1) | 5.028(1) |
| *b* | 8.799(1) | 8.986(1) | 9.019(1) | - |
| *c* | 8.309(1) | 8.418(1) | 8.391(1) | 7.466(1) |
| β (°) | 90.51(1) | 90.22(1) | 90.12(1) | - |
| *V* (Å³) | 570.98(2) | 605.10(6) | 612.22(1) | 163.51(1) |
| Space group | $P2_1/c$ | $P2_1/c$ | $P2_1/c$ | *P*6/*mmm* |
| Z | 4 | 4 | 4 | 1 |
| $D_{calc}$ (g $cm^{-3}$) | 2.885 | 3.244 | 4.504 | 3.507 |
| Absorption coefficient ($mm^{-1}$) | 1.666 | 9.443 | 28.086 | 6.567 |
| *F*(000) | 488 | 560 | 736 | 158 |
| Radiation | | Mo*K*α | | |
| 2θmax (°) | 57.17 | 60.84 | 58.07 | 58.18 |
| Reflection range | -8 ≤ h ≤ 9<br>-11 ≤ k ≤ 5<br>-11 ≤ l ≤ 6 | -11 ≤ h ≤ 11<br>-12 ≤ k ≤ 12<br>-11 ≤ l ≤ 11 | -10 ≤ h ≤ 10<br>-12 ≤ k ≤ 12<br>-11 ≤ l ≤ 11 | -6 ≤ h ≤ 6<br>-6 ≤ k ≤ 6<br>-10 ≤ l ≤ 10 |
| Total no. of reflections | 2380 | 10065 | 27292 | 7393 |
| Unique reflections | 1295 | 1742 | 1589 | 120 |
| No. parameters refined | 118 | 118 | 118 | 12 |
| $R_1$, $F > 4\sigma(F)$ | 0.023 | 0.048 | 0.015 | 0.021 |
| $R_1$, all data | 0.026 | 0.060 | 0.018 | 0.021 |
| $wR_2$ ($F^2$), all data | 0.095 | 0.104 | 0.029 | 0.050 |
| GOF | 0.811 | 1.132 | 1.106 | 1.188 |
| $\Delta\sigma_{min}$, $\Delta\sigma_{max}$ (e/Å³) | –0.496, 0.334 | –0.845, 1.567 | –0.638, 0.717 | –1.774, 0.869 |

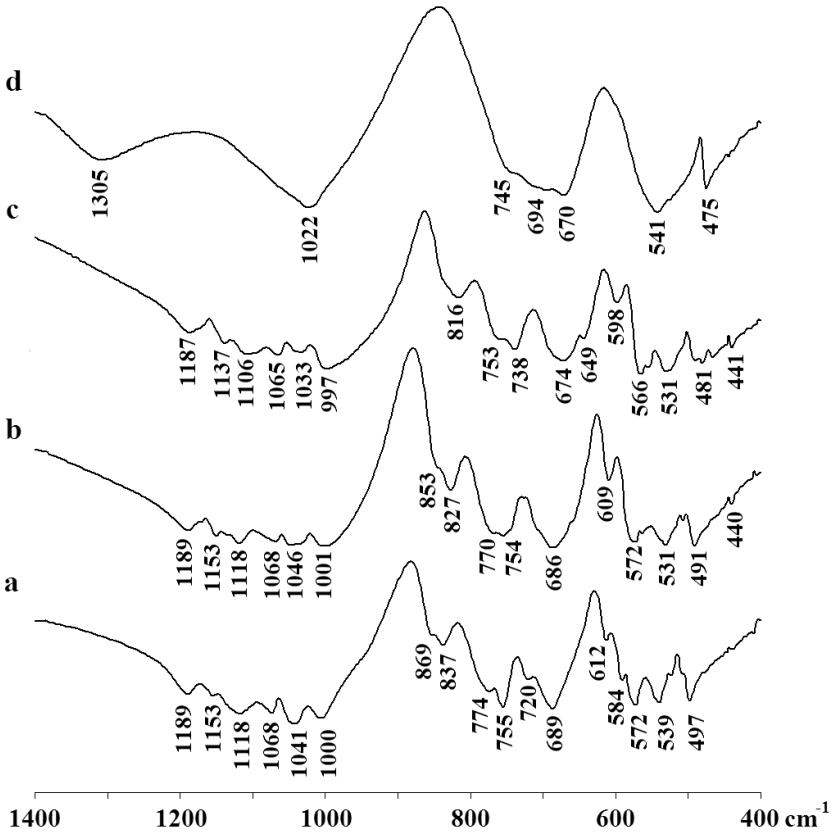


FIG. 1. Infrared spectra of (a) $CaBe_2P_2O_8$, (b) $SrBe_2P_2O_8$, (c) $PbBe_2P_2O_8$, and (d) $BaBe_2P_2O_8$.

$SrBe_2P_2O_8$ are isostructural with the minerals hurlbutite (Lindbloom *et al.* 1974) and strontiohurlbutite (Rao *et al.* 2012), respectively. Their structure consists of a framework of corner-sharing $BeO_4$ and $PO_4$ tetrahedra assembled in four- and eight-membered rings; these rings are nearly perpendicular to the *a* axis (Fig. 2a). The four-membered rings consist of a pair of tetrahedra pointing upwards (U) and a pair of tetrahedra pointing downwards (D), forming UUDD-type rings. The eight-membered rings are formed by linking four four-membered rings, and show only one pattern: DDUDUUDU (Fig. 2b). The $BeO_4$ and $PO_4$ tetrahedra are also connected by corner-sharing to form a double crankshaft chain running parallel to the *a* axis (Fig. 2c). Only linkages between $BeO_4$ and $PO_4$ tetrahedra are observed in the entire framework, and linkages such as Be–O–Be or P–O–P are strictly avoided. The divalent cations are located in the eight-membered rings and occur in distorted 7+3-coordinated polyhedron, characterized by seven short bonds and three long bonds (Fig. 3). By considering only the seven shortest bonds, this polyhedron can be described as a combination of a square pyramid and of a distorted trigonal prism, with one square face in common. The bond-valence sums for the $CaBe_2P_2O_8$, $SrBe_2P_2O_8$, and $PbBe_2P_2O_8$ compounds are given in Table 5; the parameters of Brown & Altermatt (1985) were used for Ca, Sr, P, and Be, whereas the parameters of Krivovichev & Brown (2001) were used for Pb. The bond valence sums for cations are very close to the ideal values, thus confirming the cationic distribution determined for these compounds.

### *$BaBe_2P_2O_8$*

$BaBe_2P_2O_8$ showed a structure completely different from those of the other beryllophosphates investigated in this study, but similar to that of the recently described species minjiangite (Rao *et al.* 2013, 2014). The structure of $BaBe_2P_2O_8$ is based on a double layer of tetrahedra containing both Be and P in a disordered distribution with a 1:1 ratio. The tetrahedra are characterized by one short (Be,P)–O(1) bond of 1.549(2) Å

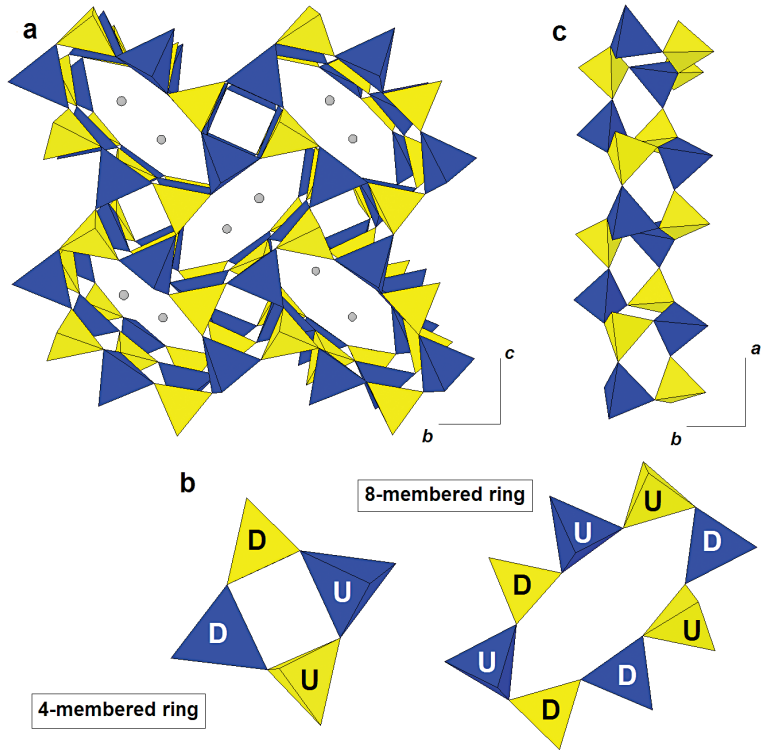


FIG. 2. The crystal structure of $M^{2+}Be_2P_2O_8$ ($M^{2+}$ = Ca, Sr, Pb) beryllophosphates. (a) View nearly perpendicular to the *a* axis. (b) Detailed view of the four- and eight-membered rings with tetrahedra pointed upward (U) and downward (D). (c) Detailed view of the double crankshaft chain running parallel to the *a* axis. $PO_4$ tetrahedra are yellow, $BeO_4$ are blue and $M^{2+}$ atoms are represented by grey spheres.

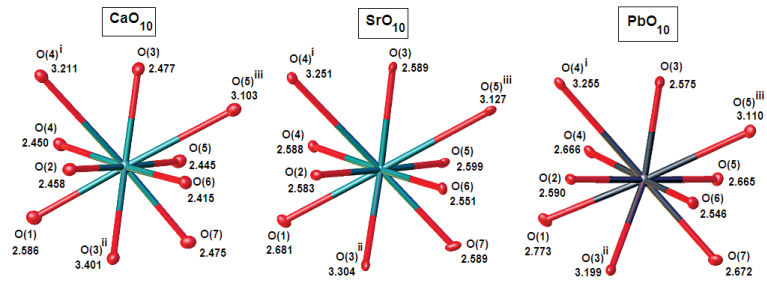


FIG. 3. Coordination of the $M^{2+}$ cation in the $CaBe_2P_2O_8$, $SrBe_2P_2O_8$, and $PbBe_2P_2O_8$ compounds. Symmetry codes: i: +x, 3/2–y, –1/2+z; ii: 1–x, 1–y, –z; iii: 2–x, 1–y, –z.

length, and by three long (Be,P)–O(2) equivalent bonds of 1.569(1) Å length. These tetrahedra are assembled in six-membered rings forming channels parallel to the *c* axis. In the *a*-*b* plane, each ring is connected to six surrounding rings to form an infinite layer (Fig. 4a). In the *c* direction, the tetrahedra are also linked by their O(1) apical oxygen atoms, thus forming a double layer with all tetrahedra of the same layer pointing in one direction (Fig. 4b). These double layers are connected by the Ba atoms, located in twelve-coordinated poly-

hedra. The Ba atoms are connected to the O(2) atoms by twelve indentical bonds 2.975(2) Å in length. The refinement of the site occupancy factors indicates that the Ba site is fully occupied, and that the tetrahedral site is statistically occupied by P and Be in a 1:1 ratio. The bond-valence sums calculated using the empirical parameters of Brown & Altermatt (1985) are 1.86 and 3.35 *vu* for the Ba and tetrahedral sites, respectively; these values are close to the theoretical values of 2 and 3.5.

## Infrared Spectroscopy

The infrared spectra of the $M^{2+}Be_2P_2O_8$ beryllophosphates are shown on Figure 1, and the assignment of their absorption bands are given in Table 6. According to the fundamental vibrational frequencies of the $PO_4$ tetrahedron (Farmer 1974), the absorption bands between 997 and 1153 $cm^{-1}$ can be attributed to $\nu_3$, the antisymmetric stretching modes of the $PO_4$ anions, and the bands between 531 and 539 $cm^{-1}$ to $\nu_4$, their bending mode. A comparison with the infrared spectra of orthophosphates of the alluaudite supergroup (Hatert *et al*. 2003, 2005a, 2005b, 2006, Hatert 2008, Kacimi *et al*. 2005, Rondeux & Hatert 2010) shows the presence of strong absorption bands between *ca*. 650 and 900 $cm^{-1}$ in the spectra of $M^{2+}Be_2P_2O_8$ (Fig. 1), bands which are absent in alluaudite-type phosphates. According to Farmer (1974), the absorption in the 700–850 $cm^{-1}$ region is distinctive for beryllium phosphates and silicates; consequently, the bands between 649 and 869 $cm^{-1}$, in the spectra of the studied compounds, were assigned to $\nu_4$, the bending mode of $BeO_4$ tetrahedra (Table 6). The bands between 1108 and 1189 $cm^{-1}$ occur at a very high wavenumber, compared to the $\nu_3$ $PO_4$ bands; they are assigned to the $\nu_3$ antisymmetric stretching vibrations of the $BeO_4$ tetrahedra. As mentioned by Farmer (1974), however, some of these bands are certainly affected by a strong coupling between the vibrational frequencies of the $BeO_4$ and $PO_4$ tetrahedra (Table 6).

The 481–612 $cm^{-1}$ region contains several absorption bands which can be attributed to the $\nu_4$ $PO_4$ bending vibration mode or to the vibrations of the $M^{2+}$–O bonds. As shown in Table 4, the *M*–O distances show a significant increase when Ca is replaced by Sr and Pb in the

TABLE 3. ATOM COORIDNATES AND ANISOTROPIC DISPLACEMENT PARAMETERS (Å²)

| | $CaBe_2P_2O_8$ | | | | | | | | | |
|---|---|---|---|---|---|---|---|---|---|---|
| | *x* | *y* | *z* | $U_{11}$ | $U_{22}$ | $U_{33}$ | $U_{23}$ | $U_{13}$ | $U_{12}$ | $U_{eq}$ |
| Ca | 0.2560(1) | 0.0856(1) | 0.1133(1) | 0.0133(2) | 0.0116(2) | 0.0149(2) | 0.0002(1) | -0.0006(1) | -0.0004(1) | 0.0132(1) |
| P(1) (T1m) | 0.0608(1) | 0.4178(1) | 0.2378(1) | 0.0094(2) | 0.0100(3) | 0.0095(2) | 0.0003(2) | -0.0001(2) | 0.0002(2) | 0.0096(1) |
| P(2) (T2o) | 0.5612(1) | 0.3019(1) | -0.0589(1) | 0.0100(2) | 0.0090(2) | 0.0098(2) | -0.0001(2) | -0.0001(2) | -0.0004(2) | 0.0096(1) |
| Be(1) (T2m) | -0.0709(3) | 0.3052(3) | -0.0552(3) | 0.0141(1) | 0.0118(1) | 0.0112(1) | -0.0004(1) | -0.0006(9) | -0.0008(1) | 0.0124(5) |
| Be(2) (T1o) | 0.5700(3) | -0.0777(3) | 0.2674(3) | 0.0129(1) | 0.0127(1) | 0.0133(1) | -0.0010(1) | 0.0006(9) | 0.0010(1) | 0.0130(5) |
| O(1) | 0.0043(2) | 0.0740(2) | 0.3131(2) | 0.0162(7) | 0.0097(7) | 0.0133(7) | -0.0010(5) | 0.0012(5) | -0.0011(5) | 0.0131(3) |
| O(2) | 0.0641(2) | 0.3067(2) | 0.0969(2) | 0.0129(6) | 0.0116(7) | 0.0115(6) | -0.0005(6) | -0.0012(5) | 0.0014(5) | 0.0120(3) |
| O(3) | 0.2408(2) | 0.4214(2) | 0.3155(2) | 0.0104(6) | 0.0186(8) | 0.0120(7) | -0.0008(6) | -0.0009(5) | -0.0003(6) | 0.0136(3) |
| O(4) | -0.0625(2) | 0.3672(2) | 0.3713(2) | 0.0136(6) | 0.0107(7) | 0.0117(7) | 0.0013(6) | 0.0025(5) | 0.0013(6) | 0.0120(3) |
| O(5) | 0.4434(2) | -0.1368(2) | 0.1223(2) | 0.0141(6) | 0.0099(7) | 0.0133(7) | -0.0015(6) | -0.0021(5) | 0.0008(5) | 0.0125(3) |
| O(6) | 0.4320(2) | 0.3089(2) | 0.0792(2) | 0.0122(6) | 0.0134(7) | 0.0113(6) | -0.0003(6) | 0.0014(5) | -0.0014(5) | 0.0123(3) |
| O(7) | 0.4977(2) | 0.0893(2) | 0.3080(2) | 0.0161(7) | 0.0105(7) | 0.0120(7) | -0.0012(5) | -0.0016(5) | 0.0011(6) | 0.0129(3) |
| O(8) | 0.7387(2) | 0.3447(2) | -0.0010(2) | 0.0104(6) | 0.0148(7) | 0.0158(7) | -0.0036(6) | 0.0004(5) | -0.0003(6) | 0.0137(3) |
| | $SrBe_2P_2O_8$ | | | | | | | | | |
| | *x* | *y* | *z* | $U_{11}$ | $U_{22}$ | $U_{33}$ | $U_{23}$ | $U_{13}$ | $U_{12}$ | $U_{eq}$ |
| Sr | 1.2555(1) | 0.0874(1) | 1.1088(1) | 0.0067(2) | 0.0072(2) | 0.0105(2) | 0.0008(2) | -0.0002(2) | -0.0005(2) | 0.0081(2) |
| P(1) (T1m) | 1.0621(1) | 0.0854(1) | 0.7319(1) | 0.0047(5) | 0.0063(5) | 0.0061(6) | 0.0002(5) | 0.0001(4) | -0.0006(4) | 0.0057(2) |
| P(2) (T2o) | 0.5636(1) | 0.1959(1) | 0.4336(1) | 0.0047(5) | 0.0039(6) | 0.0060(7) | 0.0009(4) | -0.0001(4) | 0.0005(4) | 0.0048(2) |
| Be(1) (T2m) | 0.9261(8) | 0.1937(7) | 0.4363(8) | 0.007(3) | 0.009(3) | 0.008(3) | 0.003(2) | 0.000(2) | 0.002(2) | 0.008(1) |
| Be(2) (T1o) | 0.4292(8) | 0.4187(7) | 0.2262(8) | 0.007(3) | 0.007(3) | 0.009(3) | 0.003(2) | -0.002(2) | -0.001(2) | 0.008(1) |
| O(1) | 0.9939(5) | 0.0726(4) | 0.3061(4) | 0.014(2) | 0.006(2) | 0.010(2) | -0.001(1) | 0.004(1) | -0.001(1) | 0.0099(7) |
| O(2) | 1.0556(4) | 0.1878(4) | 0.5871(4) | 0.009(2) | 0.008(2) | 0.008(2) | 0.001(1) | -0.001(1) | -0.002(1) | 0.0084(7) |
| O(3) | 0.2410(4) | 0.4075(4) | 0.3016(4) | 0.004(2) | 0.015(2) | 0.008(2) | 0.001(2) | -0.001(1) | 0.002(2) | 0.0093(7) |
| O(4) | 0.9446(4) | 0.1375(4) | 0.8649(4) | 0.008(2) | 0.007(2) | 0.009(2) | 0.001(1) | 0.002(1) | -0.001(1) | 0.0078(7) |
| O(5) | 0.5491(4) | 0.3570(4) | 0.3719(4) | 0.009(2) | 0.005(2) | 0.008(2) | 0.003(1) | -0.003(1) | 0.000(1) | 0.0079(7) |
| O(6) | 0.4372(4) | 0.3177(4) | 0.0697(4) | 0.006(1) | 0.009(2) | 0.010(2) | -0.001(1) | 0.001(1) | 0.001(1) | 0.0083(7) |
| O(7) | 0.4906(5) | 0.5880(4) | 0.1993(4) | 0.015(2) | 0.006(2) | 0.008(2) | 0.001(1) | -0.005(1) | -0.001(1) | 0.0095(7) |
| O(8) | 0.7384(4) | 0.1629(4) | 0.4921(5) | 0.007(2) | 0.012(2) | 0.015(2) | 0.003(1) | -0.001(1) | 0.001(1) | 0.0113(7) |

TABLE 3. CONTINUED

| | $PbBe_2P_2O_8$ | | | | | | | | | |
|---|---|---|---|---|---|---|---|---|---|---|
| | *x* | *y* | *z* | $U_{11}$ | $U_{22}$ | $U_{33}$ | $U_{23}$ | $U_{13}$ | $U_{12}$ | $U_{eq}$ |
| Pb | 0.7562(1) | 0.5927(1) | 0.1061(1) | 0.0113(1) | 0.0103(1) | 0.0135(1) | 0.0002(1) | 0.0004(4) | -0.0006(5) | 0.0117(1) |
| P(1) (T1m) | 0.5637(1) | 0.9135(1) | 0.2313(1) | 0.0063(4) | 0.0056(4) | 0.0071(3) | 0.0001(3) | 0.0005(3) | 0.0002(3) | 0.0063(1) |
| P(2) (T2o) | 0.9338(1) | 0.1969(1) | 0.0675(1) | 0.0068(4) | 0.0040(3) | 0.0077(3) | -0.0001(3) | 0.0002(3) | -0.0004(3) | 0.0061(1) |
| Be(1) (T2m) | 0.5761(5) | 0.1935(4) | 0.0641(5) | 0.008(2) | 0.009(2) | 0.009(2) | -0.002(1) | -0.001(1) | 0.001(1) | 0.0087(8) |
| Be(2) (T1o) | 1.0725(5) | 0.4184(5) | 0.2730(5) | 0.005(2) | 0.011(2) | 0.101(2) | 0.001(1) | 0.001(1) | 0.001(1) | 0.0089(8) |
| O(1) | 0.5175(3) | 1.0730(2) | 0.1966(3) | 0.014(1) | 0.004(1) | 0.011(1) | 0.0015(8) | 0.0040(9) | 0.0021(9) | 0.0099(5) |
| O(2) | 0.5554(3) | 0.8154(2) | 0.0834(2) | 0.009(1) | 0.009(1) | 0.008(1) | -0.0019(8) | 0.0004(8) | 0.0017(9) | 0.0089(4) |
| O(3) | 0.7412(3) | 0.8980(2) | 0.2997(3) | 0.006(1) | 0.018(1) | 0.009(1) | -0.0004(9) | 0.0004(9) | -0.0010(9) | 0.0111(5) |
| O(4) | 0.5538(3) | 0.3612(2) | 0.1369(3) | 0.011(1) | 0.007(1) | 0.010(1) | -0.0023(8) | 0.0038(9) | 0.0000(9) | 0.0094(4) |
| O(5) | 0.9533(3) | 0.3570(2) | 0.1299(3) | 0.009(1) | 0.006(1) | 0.013(1) | -0.0003(9) | -0.0012(9) | 0.0020(9) | 0.0095(4) |
| O(6) | 0.9375(3) | 0.8204(2) | 0.0666(3) | 0.008(1) | 0.008(1) | 0.011(1) | -0.0015(9) | 0.0018(9) | -0.0025(8) | 0.0093(4) |
| O(7) | 1.0203(3) | 0.5885(2) | 0.2978(3) | 0.014(1) | 0.008(1) | 0.010(1) | -0.0023(9) | -0.0017(9) | 0.0005(9) | 0.0107(5) |
| O(8) | 0.7621(3) | 0.1689(2) | 0.0045(3) | 0.008(1) | 0.012(1) | 0.012(1) | -0.0050(9) | 0.0001(9) | -0.0008(9) | 0.0106(5) |
| | $BaBe_2P_2O_8$ | | | | | | | | | |
| | *x* | *y* | *z* | $U_{11}$ | $U_{22}$ | $U_{33}$ | $U_{23}$ | $U_{13}$ | $U_{12}$ | $U_{eq}$ |
| Ba | 1 | 1 | 1 | 0.0085(3) | 0.0085(3) | 0.0087(4) | 0.000 | 0.000 | 0.0043(1) | 0.0086(3) |
| P(1)* | 0.3333 | 0.6667 | 0.7075(3) | 0.0079(8) | 0.0079(8) | 0.007(1) | 0.000 | 0.000 | 0.0040(4) | 0.0075(5) |
| Be(1)* | 0.3333 | 0.6667 | 0.7075(3) | 0.0079(8) | 0.0079(8) | 0.007(1) | 0.000 | 0.000 | 0.0040(4) | 0.0075(5) |
| O(1) | 0.3333 | 0.6667 | 0.5 | 0.012(2) | 0.012(2) | 0.018(3) | 0.000 | 0.000 | 0.0061(1) | 0.014(1) |
| O(2) | 0.5 | 0.5 | 0.7871(5) | 0.043(2) | 0.043(2) | 0.009(1) | 0.000 | 0.000 | 0.0038(2) | 0.024(1) |

*site occupancy was constrained to 0.5 P and 0.5 Be.

studied compounds. This increase, as well as the very high atomic weights of Sr and Pb, is responsible for the significant shift of the bands at 612 and 497 $cm^{-1}$ towards lower wavenumbers (Table 6). These bands are consequently assigned to the $M^{2+}$–O vibrations, while the band at 539 $cm^{-1}$, characterized by a smaller shift, is assigned to $PO_4$ vibrations.

The infrared spectrum of $BaBe_2P_2O_8$ is significantly different from those of the hurlbutite-type beryllophosphates, since its absorption bands are extremely broad (Fig. 1). This broadening is due to the disordered distribution of P and Be at the unique tetrahedral site of the crystal structure. These broad bands can easily be assigned by comparison with the assignment previously described, with $M^{2+}$–O at 475 $cm^{-1}$, $\nu_4$ $PO_4$ at 541 $cm^{-1}$, $\nu_4$ $BeO_4$ at 670, 694, 745 $cm^{-1}$, $\nu_3$ $PO_4$ at 1022 $cm^{-1}$, and $\nu_3$ $BeO_4$ at 1305 $cm^{-1}$.

## Stability Fields of $M^{2+}Be_2P_2O_8$ Compounds

The very low number of occurrences of natural beryllophosphates indicate that the conditions necessary for their formation are very uncommon. Kampf *et al*. (1992) attributed the paucity of beryllophosphate minerals to several factors, such as the requirement for nearby sources of P and Be, the resistance of beryl to alteration at the low temperatures where the beryllophosphate minerals crystallize, and the behavior of Be in aqueous solution, which is very sensitive to pH. The work of Harvey & Meier (1989) on beryllophosphate zeolites shows that pH is a critical parameter for the synthesis of this kind of compound. If the pH is below 4, the synthesized compounds are dense beryllophosphates containing neither cations nor water, and if the pH exceeds 7 no crystalline products are obtained. Moreover, it was demonstrated that using different types of alkali cations can lead to the formation of different types of zeolite structures.

In order to determine if synthetic hurlbutite, $CaBe_2P_2O_8$, is sensitive to pH variations, experiments at 200 °C were performed in a weakly basic solution (pH around 9), by using $NH_4H_2PO_4$ instead of $H_3PO_4$ as a source of P (experiments CaBeP200-3, CaBeP200-8, CaBeP200-4, and CaBeP200-7; Table 1). The comparison between these syntheses, in which the Ca:Be:P ratio is the same, indicates that the hurlbutite-type compound $CaBe_2P_2O_8$ can crystallize in a very strong acidic solution (pH = 1) as well as in a weakly basic solution (pH = 9). The crystals of $CaBe_2P_2O_8$ are the same size in both cases and synthetic hydroxylapatite occurs, in association with $CaBe_2P_2O_8$, in the experiments at pH = 9. According to the observations of Harvey & Meier (1989), it is not common to crystallize beryllophosphates with a dense structure from a solution with a pH above 7. However, the synthesis processes used in this study and in that of Harvey & Meier (1989) are different, since in the present case, the pH was not modified by the addition of tetraethyammonium hydroxide (TEAOH) solution, which leads to the formation of a gel.

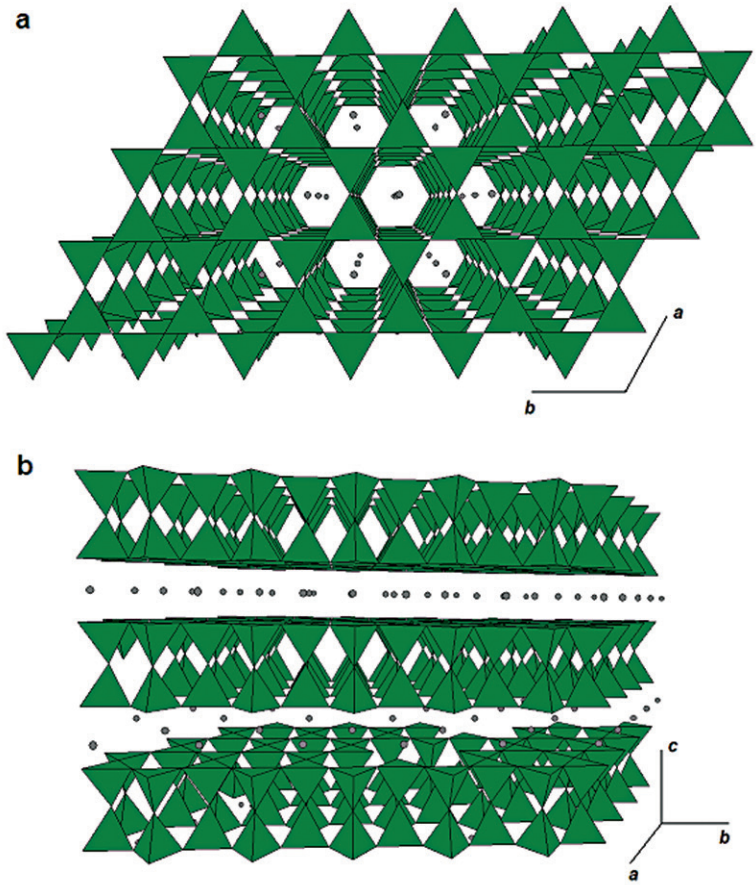


FIG. 4. The crystal structure of $BaBe_2P_2O_8$. (a) The *a*-*b* projection showing the six-membered rings. (b) View parallel to the *c* axis showing the stacking of the double layers of tetrahedra. $(Be,P)O_4$ tetrahedra are green and Ba atoms are represented by grey spheres.

Hydrothermal synthesis experiments were also performed at 400 and 600 °C and 1 kbar (Table 1). The X-ray powder diffraction patterns of the resulting products show that the $M^{2+}Be_2P_2O_8$ compounds ($M^{2+}$ = Ca, Sr, Pb, Ba) remain stable at these high temperatures and pressures. This observation is in good agreement with the comments provided in the ICDD database, which indicate that $SrBe_2P_2O_8$ and $BaBe_2P_2O_8$ were synthesized from oxides by solid-state reaction in air at 1000 °C.

## DISCUSSION

### *Crystal chemistry of $M^{2+}Be_2P_2O_8$*

As previously mentioned, the $M^{2+}$ cation in the $M^{2+}Be_2P_2O_8$ beryllophosphates ($M^{2+}$ = Ca, Sr, Pb) occurs at a site with a 7+3 coordination number. As shown in Table 4 and Figure 3, the seven shortest $M^{2+}$–O bonds are quite similar for the $CaO_7$ and $SrO_7$ polyhedra, with average values of 2.472(1) and 2.597(4) Å, respectively. This increase is in good agreement with the increase of the ionic radius between $Ca^{2+}$ (1.06 Å) and $Sr^{2+}$ (1.21 Å) in sevenfold coordination (Shannon 1976). In contrast, the seven shortest Pb–O distances show a spread between 2.546(2) and 2.773(2) Å, indicating a more distorted polyhedron with an average Pb–O bond length of 2.641(2) Å. The Pb–O1, Pb–O4, Pb–O5, and Pb–O7 bonds are the most affected by the distortion, with an increase of 0.07–0.09 Å, in comparison with the Sr–O bond lengths. The Pb–O3 bond, which points in the opposite direction from the O1, O4, O5, and O7 atoms, shows a sharp decrease in length of 0.1 Å. This pattern of deformation of the Pb

TABLE 4. INTERATOMIC DISTANCES AND ANGLES FOR $CaBe_2P_2O_8$, $SrBe_2P_2O_8$, AND $PbBe_2P_2O_8$

| | T–O distances (Å) | | | | O–T–O angles (°) | | |
|---|---|---|---|---|---|---|---|
| | CaBeP | SrBeP | PbBeP | | CaBeP | SrBeP | PbBeP |
| P(1)–O(1) | 1.523(1) | 1.523(4) | 1.515(2) | O(1)–P(1)–O(2) | 111.9(1) | 112.6(2) | 112.6(1) |
| P(1)–O(2) | 1.525(1) | 1.528(4) | 1.525(2) | O(1)–P(1)–O(3) | 113.5(1) | 112.9(2) | 112.6(1) |
| P(1)–O(3) | 1.542(1) | 1.546(4) | 1.551(2) | O(1)–P(1)–O(4) | 104.5(1) | 104.9(2) | 106.1(1) |
| P(1)–O(4) | 1.540(1) | 1.538(4) | 1.534(2) | O(2)–P(1)–O(3) | 108.2(1) | 107.8(2) | 106.7(1) |
| | | | | O(2)–P(1)–O(4) | 112.4(1) | 112.2(2) | 112.5(1) |
| <P(1)–O> | 1.532(1) | 1.534(4) | 1.531(2) | O(3)–P(1)–O(4) | 106.1(1) | 106.2(2) | 106.3(1) |
| P(2)–O(5) | 1.545(1) | 1.543(4) | 1.544(2) | O(5)–P(2)–O(6) | 106.2(1) | 106.1(2) | 105.8(1) |
| P(2)–O(6) | 1.536(1) | 1.536(4) | 1.543(2) | O(5)–P(2)–O(7) | 109.4(1) | 109.0(2) | 108.7(1) |
| P(2)–O(7) | 1.542(1) | 1.542(4) | 1.539(2) | O(5)–P(2)–O(8) | 111.2(2) | 111.3(2) | 111.8(1) |
| P(2)–O(8) | 1.510(1) | 1.510(4) | 1.507(2) | O(6)–P(2)–O(7) | 107.5(1) | 107.9(2) | 108.0(1) |
| | | | | O(6)–P(2)–O(8) | 111.1(1) | 110.7(2) | 110.5(1) |
| <P(2)–O> | 1.533(1) | 1.533(4) | 1.533(2) | O(7)–P(2)–O(8) | 111.2(1) | 111.8(2) | 111.8(1) |
| Be(1)–O(1) | 1.639(3) | 1.638(8) | 1.626(5) | O(1)–Be(1)–O(2) | 106.1(1) | 106.7(4) | 107.2(3) |
| Be(1)–O(2) | 1.639(3) | 1.636(7) | 1.632(4) | O(1)–Be(1)–O(4) | 109.6(1) | 109.8(4) | 109.2(3) |
| Be(1)–O(4) | 1.637(3) | 1.638(7) | 1.642(4) | O(1)–Be(1)–O(8) | 112.8(2) | 113.2(4) | 113.4(3) |
| Be(1)–O(8) | 1.595(3) | 1.599(7) | 1.602(5) | O(2)–Be(1)–O(4) | 105.5(1) | 104.9(4) | 104.8(3) |
| | | | | O(2)–Be(1)–O(8) | 112.0(1) | 111.0(4) | 111.6(3) |
| <Be(1)–O> | 1.627(3) | 1.627(7) | 1.625(5) | O(4)–Be(1)–O(8) | 110.4(1) | 110.8(4) | 110.3(3) |
| Be(2)–O(3) | 1.636(3) | 1.639(7) | 1.637(5) | O(3)–Be(2)–O(5) | 103.3(1) | 102.9(4) | 103.3(3) |
| Be(2)–O(5) | 1.638(3) | 1.650(7) | 1.635(5) | O(3)–Be(2)–O(6) | 110.1(1) | 108.9(4) | 107.3(3) |
| Be(2)–O(6) | 1.619(3) | 1.601(8) | 1.612(5) | O(3)–Be(2)–O(7) | 114.3(2) | 113.1(4) | 113.5(3) |
| Be(2)–O(7) | 1.611(3) | 1.614(7) | 1.605(4) | O(5)–Be(2)–O(6) | 111.9(2) | 113.3(4) | 113.4(3) |
| | | | | O(5)–Be(2)–O(7) | 103.5(1) | 104.1(4) | 105.3(3) |
| <Be(2)–O> | 1.626(3) | 1.626(7) | 1.622(5) | O(6)–Be(2)–O(7) | 113.1(2) | 113.9(4) | 113.7(3) |

M–O distances (Å) (M = Ca, Sr, Pb)

| | CaBeP | SrBeP | PbBeP |
|---|---|---|---|
| *M*–O(1) | 2.586(1) | 2.681(4) | 2.773(2) |
| *M*–O(2) | 2.458(1) | 2.583(4) | 2.590(2) |
| *M*–O(3) | 2.477(1) | 2.589(4) | 2.575(2) |
| *M*–O(4) | 2.450(1) | 2.588(3) | 2.666(2) |
| *M*–O(5) | 2.445(1) | 2.599(4) | 2.665(2) |
| *M*–O(6) | 2.415(1) | 2.551(3) | 2.546(2) |
| *M*–O(7) | 2.475(1) | 2.589(4) | 2.672(2) |
| <*M*–O> [7] | 2.472(1) | 2.597(4) | 2.641(2) |
| *M*–O(3) | 3.401(1) | 3.304(4) | 3.199(2) |
| *M*–O(4) | 3.211(1) | 3.251(4) | 3.255(2) |
| *M*–O(5) | 3.103(1) | 3.127(4) | 3.110(2) |
| <*M*–O> [10] | 2.702(1) | 2.786(4) | 2.805(2) |

CaBeP for $CaBe_2P_2O_8$, SrBeP for $SrBe_2P_2O_8$ and PbBeP for $PbBe_2P_2O_8$

polyhedron can be explained by the the presence of the $Pb^{2+}$ lone-pair electrons, which creates a shift in the position of the Pb atom from the center of the cavity. Benna *et al*. (1996) observed the same kind of distortion for the Pb polyhedron in the synthetic ordered and disordered lead feldspar $PbAl_2Si_2O_8$.

Figure 5a shows the correlation between the ionic radius of the $M^{2+}$ cation and the average $M^{2+}$–O bond length, for seven- and 10-fold coordination. In both the cases, the most significant increase in the $M^{2+}$–O bond length is between the Ca and Sr compounds; indeed, the difference between the ionic radius of $Sr^{2+}$

(1.21 Å) and $Pb^{2+}$ (1.23 Å) in sevenfold coordination (Shannon 1976) is quite low. The unit-cell parameters are also affected by the nature of the cation located at the *M* site (Fig. 5b): as for the $M^{2+}$–O bond lengths, the most significant variations occur between the Ca and Sr-bearing compounds, due to the large variation in the ionic radii of $Ca^{2+}$ and $Sr^{2+}$. Comparison between *CaBeP* and *SrBeP* shows that the unit-cell volume increases by 5.97%; the unit-cell volume of *PbBeP* increases by 7.22% when compared to that of *CaBeP* (Fig. 5b, Table 2).

*Structural comparison with silicate analogues*

$CaBe_2P_2O_8$, $SrBe_2P_2O_8$, and $PbBe_2P_2O_8$ have a typical paracelsian-type structure, characterized by four-membered and eight-membered rings showing only the UUDD and DDUDUUDU patterns, respectively (Smith 1953, Smith & Rinaldi 1962). The paracelsian structure is similar to the orthoclase structure, but differs slightly in the orientation of the double crankshaft chains. In both cases, the four-membered rings show the pattern UUDD, but the rotation of the crankshaft chains in orthoclase leads to the formation of two kinds of eight-membered rings: one type showing the DDUDUUDU pattern (as in paracelsian), and a second type showing the UUUUDDDD pattern (Fig. 6c). Figure 6 also shows that the paracelsian structure is topologically identical to the structure of the $M^{2+}B_2Si_2O_8$ borosilicates ($M^{2+}$ = Ca, Sr, Ba), in which only the eight-membered ring with the DDUDUUDU pattern is observed (Fig. 6a and 6b; Phillips *et al.* 1974, Pautov *et al.* 2004). However, the ordering scheme of cations at the tetrahedral sites constituting the double crankshaft chain is different in borosilicates: as shown in Figure 7, a perfect alternation between $BeO_4$ and $PO_4$ tetrahedra is observed in the paracelsian structure (Fig. 7a), whereas connections between $BO_4$ and $SiO_4$ tetrahedra occur in $M^{2+}B_2Si_2O_8$ borosilicates, thus leading to the formation of $B_2O_7$ and $Si_2O_7$ groups (Fig. 7b).

The bond-angle distortion of tetrahedra was calculated using the $\sigma_{tet}$ parameter of Baur (1974) (Table 7). As previously mentioned by Phillips *et al.* (1975) and

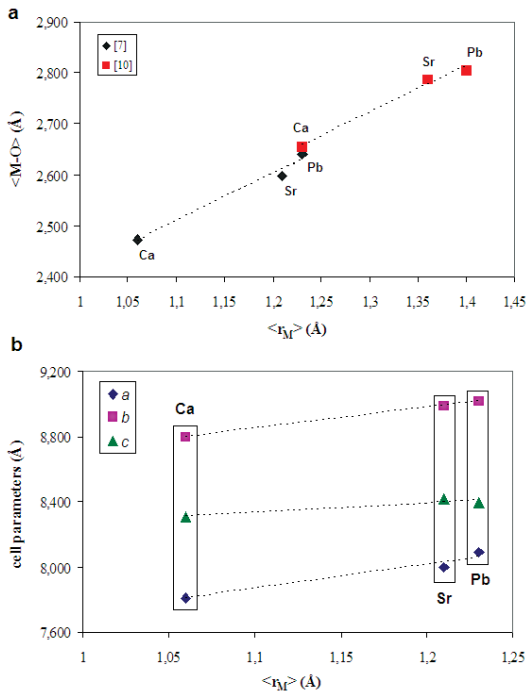


FIG. 5. Variations of (a) the mean $M^{2+}$–O bond lengths and (b) the unit-cell parameters as a function of the ionic radius of the $M^{2+}$ cation in the synthetic $M^{2+}Be_2P_2O_8$ beryllophosphates.

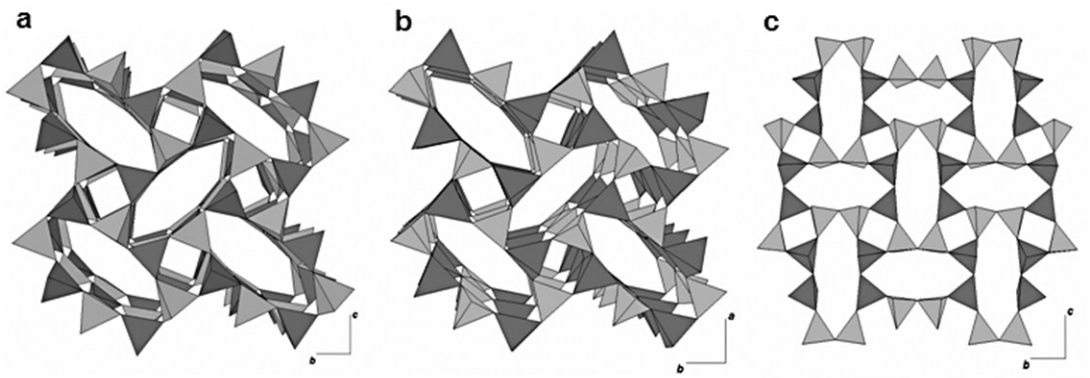


FIG. 6. Comparison between the structures of (a) $CaBe_2P_2O_8$ (hurlbutite), (b) $CaB_2Si_2O_8$ (danburite), and (c) $KAlSi_3O_8$ (orthoclase). Views perpendicular to the crankshaft chain axis.

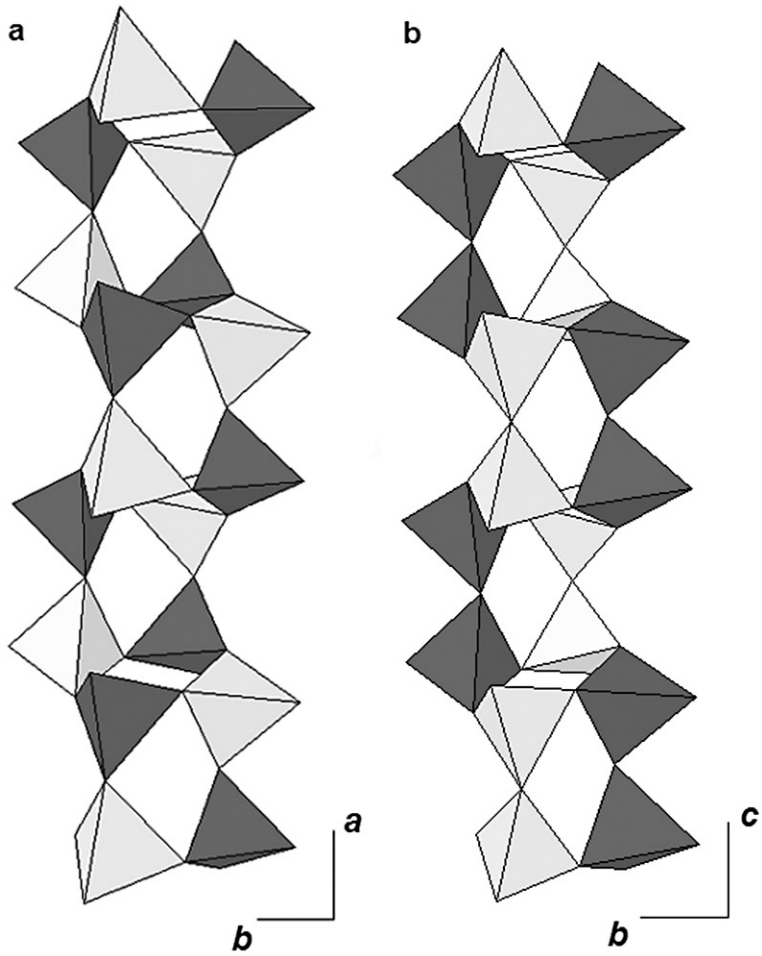


FIG. 7. Comparison between the double crankshaft chains in (a) beryllophosphates and (b) borosilicates.

Lucas *et al*. (1998), the *T*1 (P1 and Be2) and *T*2 (P2 and Be1) sites are not structurally equivalent in the paracelsian structure type. The $T1O_4$ tetrahedra always share more O atoms with the $M^{2+}O_7$ polyhedra than the $T2O_4$ tetrahedra and, as a result, the $T1O_4$ tetrahedra are always more distorted than the $T2O_4$ tetrahedra. This feature is shown in Table 7 by a $\sigma_{T2}/\sigma_{T1}$ ratio that is always lower than 1. The distortion coefficient is also influenced by the charge and the ionic radius of the tetrahedrally coordinated cations: the higher the charge and the smaller the radius, the more the tetrahedrally coordinated cation becomes polarized in its anionic environnment. Consequently, the distortion should decrease when the bond length increases (Lucas *et al*. 1998). However, despite the replacement of Ca by Sr or Pb in the $M^{2+}Be_2P_2O_8$ beryllophosphates, the distortion parameters are very constant for the four distinctive tetrahedra occurring in the structure (Table 7). These parameters are also very low, in comparison with those of other compounds showing a paracelsian-type structure; this feature cannot be explained satisfactorily. The

TABLE 5. BOND-VALENCES SUMS (*vu*) FOR $CaBe_2P_2O_8$, $SrBe_2P_2O_8$, AND $PbBe_2P_2O_8$

| | $M^{2+}$ | P(1) | P(2) | Be(1) | Be(2) |
|---|---|---|---|---|---|
| $CaBe_2P_2O_8$ | 1.90 | 5.03 | 5.02 | 2.06 | 2.06 |
| $SrBe_2P_2O_8$ | 2.08 | 5.01 | 5.02 | 2.05 | 2.06 |
| $PbBe_2P_2O_8$ | 2.02 | 5.04 | 5.02 | 2.07 | 2.08 |
| Ideal value | 2 | 5 | 5 | 2 | 2 |

ratios between the distortion parameters of tetrahedra containing Be and those containing P, around 0.8, are relatively close to 1.0, thus indicating that the $BeO_4$ and $PO_4$ tetrahedra are similarly distorted.

$BaBe_2P_2O_8$ is topologically identical to the mineral dmisteinbergite, $CaAl_2Si_2O_8$, a high-temperature polymorph of anorthite described by Chesnokov *et al*. (1990). The crystal structure of dmisteinbergite was refined by Takéuchi & Donnay (1959) from synthetic crystals. The structure of $BaBe_2P_2O_8$ is also similar to that of the synthetic hexagonal compound β-$BaAl_2Si_2O_8$ (Takéuchi 1958). Furthermore, Lucas *et al*. (1998) reported that the compounds $SrZn_2As_2O_8$ and $BaZn_2As_2O_8$, synthesized at 1060–1070 °C, show powder diffraction patterns similar to that of hexagonal celsian $BaAl_2Si_2O_8$. Finally, the work of Nedic *et al*. (2008) indicates that crystals of $SrAl_2Si_2O_8$, synthesized at 1000 °C, show a structure analogous to that of $BaBe_2P_2O_8$.

TABLE 6. ASSIGNMENT OF THE INFRARED FREQUENCIES ($cm^{-1}$) FOR THE SYNTHETIC BERYLLOPHOSPHATES

| $CaBe_2P_2O_8$ | $SrBe_2P_2O_8$ | $PbBe_2P_2O_8$ | Assignment |
|---|---|---|---|
| 1189 | 1189 | 1187 | $\nu_3$ $BeO_4$ |
| 1153 | 1153 | 1139 | $\nu_3$ $PO_4$ + $BeO_4$ ? |
| 1118 | 1118 | 1108 | $\nu_3$ $PO_4$ + $BeO_4$ ? |
| 1068 | 1068 | 1065 | $\nu_3$ $PO_4$ |
| 1041 | 1046 | 1033 | $\nu_3$ $PO_4$ |
| 1000 | 1001 | 997 | $\nu_3$ $PO_4$ |
| 869 | 853 | - | $\nu_4$ $BeO_4$ |
| 837 | 827 | 816 | $\nu_4$ $BeO_4$ |
| 774 | 770 | 753 | $\nu_4$ $BeO_4$ |
| 755 | 754 | 738 | $\nu_4$ $BeO_4$ |
| 720 | - | - | $\nu_4$ $BeO_4$ |
| 686 | 686 | 674 | $\nu_4$ $BeO_4$ |
| - | - | 649 | $\nu_4$ $BeO_4$ |
| 612 | 609 | 598 | $M^{2+}$–O |
| 584 | - | - | ? |
| 539 | 531 | 531 | $\nu_4$ $PO_4$ |
| 497 | 491 | 481 | $M^{2+}$–O |

## Acknowledgements

This paper is dedicated to André-Mathieu Fransolet, Paul Keller, and François Fontan, for their outstanding contribution to the petrography, mineralogy, and crystal chemistry of pegmatite phosphate minerals. We would like to thank particularly André-Mathieu, who was director of the Laboratory of Mineralogy, University of Liège, for more than 20 years, and incited us to discover the complex but fascinating world of phosphates. Fabrice Dal Bo thanks the FRS-F.N.R.S. (Belgium) for a FRIA PhD grant n° FC 93482.

## References

Agilent (2012) *CrysAlis PRO*. Agilent Technologies, Yarnton, Oxfordshire, England.

Baur, H.W. (1974) The geometry of polyhedral distortions. Predictive relationships for the phosphate group. *Acta Crystallographica* **B30**, 1195–1215.

Benna, P., Tribaudino, M., & Bruno, E. (1996). The structure of ordered and disordered lead feldspar ($PbAl_2Si_2O_8$). *American Mineralogist* **81**, 1337–1343.

Brown, I.D. & Altermatt, D. (1985) Bond-valence parameters obtained from a systematic analysis of the Inorganic Crystal Structure Database. *Acta Crystallographica* **B41**, 244–247.

Calleri, M. & Gazzoni, G. (1976) The structure of (Sr,Ba)[$(Al,Ga)_2(Si,Ge)_2O_8$]. III. The crystal structures of the paracelsian-like modifications of synthetic $SrGa_2Ge_2O_8$ and $BaGa_2Ge_2O_8$. *Acta Crystallographica* **B32**, 1196–1205.

Černý, P. (2002) Mineralogy of beryllium in granitic pegmatites. *In* Beryllium: Mineralogy, Petrology, and Geo-

TABLE 7. BOND ANGLE DISTORTION PARAMETERS FOR TETRAHEDRAL SITES OF PARACELSIAN-TYPE COMPOUNDS

| | *SrGaSi* | *SrGaGe* | *BaGaGe* | *BaZnP* | *BaZnAs* | *SrZnAs* | *CaBeP* | *SrBeP* | *PbBeP* |
|---|---|---|---|---|---|---|---|---|---|
| $\sigma_{T1o}$ | 5.06 | 5.60 | 5.06 | 6.36 | 5.22 | 7.06 | 3.60 | 3.71 | 3.76 |
| $\sigma_{T1m}$ | 3.32 | 4.51 | 4.58 | 2.44 | 1.22 | 2.46 | 2.89 | 2.86 | 2.83 |
| $\sigma_{T2o}$ | 1.61 | 2.06 | 2.14 | 1.83 | 1.81 | 2.13 | 1.58 | 1.64 | 1.76 |
| $\sigma_{T2m}$ | 2.79 | 2.63 | 2.71 | 4.42 | 2.93 | 4.00 | 2.17 | 2.17 | 2.14 |
| $\sigma_{(Si, Ge, P, As)}$ / $\sigma_{(Ga, Zn, Be)}$ | 0.63 | 0.80 | 0.86 | 0.40 | 0.37 | 0.42 | 0.77 | 0.76 | 0.78 |
| $\sigma_{T2}/\sigma_{T1}$ | 0.53 | 0.46 | 0.50 | 0.71 | 0.74 | 0.64 | 0.58 | 0.58 | 0.59 |

References: $SrGa_2Si_2O_8$ (*SrGaSi*) and $SrGa_2Ge_2O_8$ (*SrGaGe*): Phillips *et al*. (1975); $BaGa_2Ge_2O_8$ (*BaGaGe*): Calleri & Gazzoni (1976); $BaZn_2P_2O_8$ (*BaZnP*), $BaZn_2As_2O_8$ (*BaZnAs*), and $SrZn_2As_2O_8$ (*SrZnAs*): Lucas *et al*. (1998); *CaBeP*, *SrBeP*, and *PbBeP*: this work.

chemistry (E.S. Grew, ed.). *Reviews in Mineralogy and Geochemistry* **50**, 405–444.

Chesnokov, B.V., Lotova, E.V., Nigmatullina, E.N., Pavlutchenko, V.S., & Bushmakin, A.F. (1990) Dmisteinbergite, $CaAl_2Si_2O_8$, (hexagonal), a new mineral. *Zapiski Vsesoyuznogo Mineralogicheskogo Obshchestva* **119**, 43–46 (in Russian).

Farmer, V.C. (1974) The infrared spectra of minerals. *Mineralogical Society Monographs* **4**, 539.

Foit, F.F., Phillips, M.W., & Gibbs, G.V. (1973) A refinement of the crystal structure of datolite, $CaBSiO_4(OH)$. *American Mineralogist* **58**, 909–914.

Grigoriev, N.A. (1963) Glucine, a new beryllium mineral. *Zapiski Vsesoyuznogo Mineralogicheskogo Obshchestva* **92**, 691–696 (in Russian).

Hansen, S., Fälth, L., & Johnson, O. (1984) Bergslagite, a mineral with tetrahedral berylloarsenate sheet anions. *Zeitschrift für Kristallographie* **166**, 73–80.

Harvey, G. & Meier, W.M. (1989) The synthesis of beryllophosphate zeolites. *In* Zeolites: Facts, Figures, Future (P.A. Jacops & R.A. van Santen, eds.). Elsevier, Amsterdam, Netherlands.

Hatert, F. (2008) The crystal chemistry of the divalent cation in alluaudite-type phosphates: a structural and infrared spectral study of the $Na_{1.5}(Mn_{1-x}M^{2+}{}_x)_{1.5}Fe_{1.5}(PO_4)_3$ solid solutions (x = 0 to 1, $M^{2+} = Cd^{2+}$, $Zn^{2+}$). *Journal of Solid State Chemistry* **181,** 1258–1272.

Hatert, F., Hermann, R.P., Long, G.J., Fransolet, A.-M., & Grandjean, F. (2003) An X-ray Rietveld, infrared, and Mössbauer spectral study of the $NaMn(Fe_{1-x}In_x)_2(PO_4)_3$ alluaudite-like solid solution. *American Mineralogist* **88**, 211–222.

Hatert, F., Rebbouh, L., Hermann, R.P., Fransolet, A.-M., Long, G.J., & Grandjean, F. (2005a) Crystal chemistry of the hydrothermally synthesized $Na_2(Mn_{1-x}Fe^{2+}{}_x)_2Fe^{3+}(PO_4)_3$ alluaudite-type solid solution. *American Mineralogist* **90**, 653–662.

Hatert, F., Lefevre, P., Fransolet, A.-M., Spirlet, M.-R., Rebbouh, L., Fontan, F., & Keller, P. (2005b) Ferrorosemaryite, $NaFe^{2+}Fe^{3+}Al(PO_4)_3$, a new phosphate mineral from the Rubindi pegmatite, Rwanda. *European Journal of Mineralogy* **17**, 749–759.

Hatert, F., Hermann, R.P., Fransolet, A.-M., Long, G.J., & Grandjean, F. (2006) A structural, infrared, and Mössbauer spectral study of rosemaryite, $NaMnFe^{3+}Al(PO_4)_3$. *European Journal of Mineralogy* **18**, 775–785.

Hawthorne, F.C. & Huminicki, D. (2002) The crystal chemistry of beryllium. *In* Beryllium: Mineralogy, Petrelogy, and Geochemistry (E.S. Grew, ed.). *Reviews in Mineralogy and Geochemistry* **50**, 333–403.

ICDD (2012) *WebPDF-4*$^+$. International Centre for Diffraction Data, Newtown Square, Pennsylvania, USA.

Kacimi, M., Ziyad, M., & Hatert, F. (2005) Structural features of $AgCaCdMg_2(PO_4)_3$ and $AgCd_2Mg_2(PO_4)_3$, two new compounds with the alluaudite-type structure, and their catalytic activity in butan-2-ol conversion. *Materials Research Bulletin* **40**, 682–693.

Kampf, A.R. (1992) Beryllophosphate chains in the structure of fransoletite, parafransoletite, and ehrleite and some general comments on beryllophosphate linkages. *American Mineralogist* **77**, 848–856.

Kampf, A.R., Dunn, P.J., & Foord, E.E. (1992) Parafransoletite, a new dimorph of fransoletite from the Tip Top Pegmatite, Custer, South Dakota. *American Mineralogist* **77**, 843–847.

Krivovichev, S.V. & Brown, I.D. (2001) Are the compressive effects of encapsulation an artifact of the bound valence parameters? *Zeitschrift für Kristallographie* **216**, 245–247.

Lindberg, M.L. & Murata, K.J. (1953) Faheyite, a new phosphate mineral from the Sapucaia pegmatite mine, Minas Gerais, Brazil. *American Mineralogist* **38**, 263–270.

Lindbloom, J.T., Gibbs, G.V., & Ribbe, P.H. (1974) The crystal structure of hurlbutite: A comparison with danburite and anorthite. *American Mineralogist* **59**, 1267–1271.

Lucas, F., Elfakir, A., Wallez, G., Quarton, M., & Lagache, M. (1998) Synthesis and rietveld refinement of new phosphate and arsenate analogues of paracelsian. *Canadian Mineralogist* **36**, 1045–1051.

Nedic, B., Kremenovic, A., Dimitrijevic, R., & Dondur, V. (2008) Crystal structures of Sr-diphylloalumosilicates synthesized from LTA and FAU zeolites. *Solid State Sciences* **10**, 154–159.

Pautov, L.A., Agakhanov, A.A., Sokolova, E., & Hawthorne, F.C. (2004) Maleevite, $BaB_2Si_2O_8$, and pekovite, $SrB_2Si_2O_8$, new mineral species from the Dara-i-Pioz alkaline massif, northern Tajikistan: description and crystal structure. *Canadian Mineralogist* **42**, 107–119.

Peacor, D.R., Rouse, R.C., & Ahn, J.H. (1987) Crystal structure of tiptopite, a framework beryllophosphate isotypic with basic cancrinite. *American Mineralogist* **72**, 816–820.

Phillips, M.W., Gibbs, G.V., & Ribbe, P.H. (1974) The crystal structure of danburite: A comparison with anorthite, albite, reedmergnerite. *American Mineralogist* **59**, 79–85.

Phillips, M.W., Kroll, H., Pentinghaus, H., & Ribbe, P.H. (1975) The structures of synthetic paracelsian analogs, $SrGa_2Si_2O_8$ and $SrGa_2Ge_2O_8$. *American Mineralogist* **60**, 659–666.

Pluth, J.J. & Smith, J.V. (1972) Positions of cations and molecules in zeolites with the faujasite-type framework VII.

Dehydrated Ca-exchanged X. *Materials Research Bulletin* **7**, 1311–1322.

RAO, C., WANG, R., GU, X., HU, H., & DONG, C. (2012) Strontiohurlbutite, IMA 2012-032. *CNMNC Newsletter* **14**, 1285; *Mineralogical Magazine* **76**, 1281–1288.

RAO, C., HATERT, F., WANG, R.C., GU, X.P., DAL BO, F., & DONG, C.W. (2013) Minjiangite, IMA 2013-021. *CNMNC Newsletter* **16**, 2705. *Mineralogical Magazine* **77**, 2695–2709.

RAO, C., HATERT, F., WANG, R.C., GU, X.P., DAL BO, F., & DONG, C.W. (2014) Minjiangite, $Ba[Be_2P_2O_8]$, a new mineral from Nanping No. 31 pegmatite, Fujian Province, Southeastern China. *American Mineralogist*, submitted.

RONDEUX, M. & HATERT, F. (2010) An X-ray Rietveld and infrared spectral study of the $Na_2(Mn_{1-x}M^{2+}{}_x)Fe^{2+}Fe^{3+}(PO_4)_3$ (x = 0 to 1, $M^{2+}$ = Mg, Cd) alluaudite-type solid solutions. *American Mineralogst* **95**, 844–852.

SHANNON, R.D. (1976) Revised effective ionic radii and systematic studies of interatomic distances in halides and chalcogenides. *Acta Crystallographica* **A32**, 751–767.

SHELDRICK, G.M. (2008) A short history of *SHELX*. *Acta Crystallographica* **A64**, 112–122.

SMITH, J.V. (1953) The crystal structure of paracelsian, $BaAl_2Si_2O_8$. *Acta Crystallographica* **6**, 613–620.

SMITH, J.V. & RINALDI, F. (1962) Framework structures formed from parallel four- and eight-membered rings. *Mineralogical Magazine* **33**, 202–212.

TAKÉUCHI, Y. (1958) A detailed investigation of the structure of hexagonal $BaAl_2Si_2O_8$ with reference to its α-β inversion. *Mineralogical Journal* **2**, 311–332.

TAKÉUCHI, Y. & DONNAY, G. (1959) The crystal structure of hexagonal $CaAl_2Si_2O_8$. *Acta Crystallographica* **12**, 465-470.

TUTTLE, O.F. (1949) Two pressure vessels for silicate-water studies. *Geological Society of America Bulletin* **60**, 1727–1729.

WILSON, A.J.C. (1992) *International Tables for X-ray Crystallography, Volume C*. Kluwer Academic Press, London, 883pp.

*Received January 13, 2014. Revised manuscript accepted March 21, 2014.*